Semiclassical method for calculating quantum-lattice-fluctuation effects in conducting and/or optically active polymers, with results for polyacetylene in the soliton-antisoliton approximation

David M. Mackie
S³I Directorate, Army Research Laboratory, Adelphi, Maryland 20783

Arnold J. Glick
Department of Physics, University of Maryland, College Park, Maryland 20740
(Received 1 April 1992; revised manuscript received 13 January 1993)

Deviations from the lowest-energy configuration due to the quantum nature of the lattice—called quantum lattice fluctuations (QLF's)—may significantly affect the properties of conjugated polymers. In this paper, we present a semiclassical method for including QLF effects in calculations of conducting and/or optically active polymer properties. We then apply the method to the first- and third-order absorption intensities of pristine finite chains of *trans*- and *cis*-$(CH)_x$ containing fluctuation-induced soliton-antisoliton pairs. The first-order results agree with previous calculations, which used different methods. Third-order results indicate that QLF effects are enhanced by asymmetry, and degraded by disorder. They are most important below the three-photon peak, and remain substantial even for nondegenerate ground-state polymers.

I. INTRODUCTION

Conjugated polymers, many of which were already objects of great interest because of their unusual conducting properties, are receiving renewed attention because of their nonlinear optical properties. The large off-resonant nonlinear susceptibilities and subpicosecond response times of these materials are ideal for optoelectronic applications. (Of course, for real-life devices there are additional material considerations, such as linear transmission, processability, and environmental stability.) The archetypical conducting polymer is polyacetylene, $(CH)_x$. [For a recent review of $(CH)_x$, see Ref. 1.] Measurements[2–4] show that the magnitude of the third-order susceptibility, $\chi^{(3)}$, of $(CH)_x$ is unusually high—in fact, it is one of the highest of known materials. In addition, $\chi^{(3)}$ of $(CH)_x$ has not only a peak at around $\frac{1}{3}$ of the band-gap energy, but also a smaller peak at around $\frac{1}{2}$ of the band-gap energy. The experimental results have been reproduced, with varying degrees of agreement, in several analytical and numerical calculations. (See, for example, Refs. 5–9.)

Besides being inherently interesting, $\chi^{(3)}$ can also be useful as a probe of other aspects of optically active polymers, such as chain length[10] or disorder.[11] Previously we presented calculations[5] which indicated several areas in which $\chi^{(3)}$ studies could provide information on $(CH)_x$. It was shown that in pristine $(CH)_x$ a peak due to neutral solitons should be detectable in the third-order absorption at 0.15 eV, below the range currently resolved in experiments. (This is in contrast to the first-order case, in which the neutral soliton absorption peak is pushed into the tail of the main interband absorption peak by electron-electron interactions.[12]) It was also shown that in lightly doped $(CH)_x$ the magnitudes of the absorption peaks due to charged solitons are strongly dependent on the location of the dopant impurities along the chains.

Due to the quantum nature of the lattice, a set of conjugated polymer chains in the ground state can be found in any of a distribution of configurations about the classical ground-state configuration. Excited states may also exhibit these configurational fluctuations, which are known as quantum lattice fluctuations (QLF's). The importance of QLF effects in conducting and/or optically active polymers has been previously explored by Yu, Matsuoka, and Su.[13] They proposed that the most important QLF in $(CH)_x$ is the soliton-antisoliton pair, $S\bar{S}$. Modeling each soliton as a disturbance of the lattice order parameter which varies as the hyperbolic tangent, and fixing the soliton width, they were able to quantize the lattice in terms of a single variable—the separation of the centers of the soliton and antisoliton in the $S\bar{S}$. They calculated the first-order optical absorption of $(CH)_x$ and showed that QLF effects are able to account for the low-energy tail of the interband absorption peak. In a later paper, Sinclair *et al.*[6] used this model of QLF's in $(CH)_x$ to calculate $\chi^{(3)}$. The two peaks were duly reproduced in the correct locations, and a qualitative result was obtained for the peak height ratio, the larger peak being infinite and the smaller peak being finite.

We wished to investigate QLF effects in $(CH)_x$ further. However, even in the $S\bar{S}$ approximation, the method of Yu *et al.* becomes very cumbersome for the cases we had in mind. For instance, merely accounting for finite chain length, requiring electron-lattice self-consistency, or including electron-electron interactions, necessitates a different approach. For $(CH)_x$ chains which already have lattice distortions, such as solitons (for neutral or doped odd chains) or polarons (for doped even chains), the calculations become very complicated. Also, there is interest in QLF effects in other materials. For example, the

effect of $S\bar{S}$'s on the optical absorption and luminescence spectra for the nondegenerate-ground-state materials polythiophene and poly(3-hexylthienylene) has been investigated[14] using a modification of the method of Yu *et al.* Accordingly, in the next section we develop a more generally applicable procedure for calculating QLF effects in other conducting and/or optically active polymers.

II. ALTERNATE QUANTUM-LATTICE-FLUCTUATION CALCULATION

A general quasi-one-dimensional polymer has the Hamiltonian

$$H=\tfrac{1}{2}m\sum_n(\dot{x}_n)^2+V(\{x_n\}) , \tag{2.1}$$

where m is the site mass and V is the potential energy for a given set of x_n's. Let us consider only lattice configurations which are describable as functions of a single variable, the "configuration coordinate," h. That is, we let

$$x_n=f_n(h) , \tag{2.2}$$

where the f_n's are a set of single-valued functions. Imposing this restriction simplifies the problem considerably, while still retaining sufficient generality for our purposes. The choice of h (and, by implication, the f_n's) depends on the set of lattice configurations which one wishes to study. For example, one might choose h to characterize the degree of dimerization, or the magnitude or location along a chain of a distortion, or the distance from a chain or location along a chain of an impurity, or the distance between distortions or impurities. We discuss our chosen definition of h below. Putting Eq. (2.2) into Eq. (2.1) yields

$$H=\frac{1}{2M(h)}(p_0)^2+V(h) , \tag{2.3}$$

where $M(h)$ is defined as

$$M(h)\equiv m\sum_n[df_n(h)/dh]^2 , \tag{2.4}$$

and where the generalized momentum is given by

$$p_0=M(h)dh/dt . \tag{2.5}$$

The quantum-mechanical analog is

$$\left[\frac{-\hbar^2}{2M(h)}\frac{d^2}{dh^2}+V(h)\right]\psi(h)=E\psi(h) , \tag{2.6}$$

which can be solved numerically for the eigenvalues and eigenvectors if $M(h)$ is known. In the previous QLF investigations[6,13,14] mentioned above, the f_n's were defined according to exact or approximate $S\bar{S}$ solutions obtained for infinite chains of *trans*-$(CH)_x$. The defined f_n's were then used in Eq. (2.4) to find $M(h)$. This procedure becomes very complicated (and/or not as reasonable) for systems other than long even chains of *trans*-$(CH)_x$. Here, we assume that x_n's are determined in such a way that only the configurational coordinate h is readily available—the f_n's are unknown, so Eq. (2.4) cannot be used. Instead, we utilize dynamic lattice calculations (such as described in Appendix B) to "measure" $M(h)$ "experimentally."

Consider a linear polymer with a given lattice configuration, yielding a given value of h (which, in general, is not the classical ground-state value of h). If the system is allowed to relax dynamically for a short time Δt, there will be a change in h and a change in the system energy $V(h)$, which we will call Δh and ΔV, respectively. From Δt, Δh, and ΔV, we can calculate $M(h)$ using Newton's Second Law in the following manner: The force F_0 is

$$F_0=-\Delta V/\Delta h , \tag{2.7}$$

and expanding $h(t)$ in a Taylor series readily yields

$$a_0\cong 2\Delta h/(\Delta t)^2 \tag{2.8}$$

for the acceleration, so that the mass is given by

$$M(h)\cong-\tfrac{1}{2}\Delta V(\Delta t/\Delta h)^2 . \tag{2.9}$$

The accuracy of the approximation depends on choosing Δt small enough. When $M(h)$ and $V(h)$ are obtained at a sufficient number of h values to allow trustworthy interpolation, then Eq. (2.6) can be solved numerically for the energies and wave functions.

In order to do most calculations exactly, this process would have to be repeated for all electronic states of the system, and system wave functions would be products of properly antisymmetrized many-electron (i.e., Slater determinant) wave functions and one of the (numerous) configuration coordinate wave functions associated with that electronic state. Such a procedure would be extremely lengthy and complicated. Previous QLF investigations[6,13,14] restricted the sums over the electronic and configuration states, including only the ground and first one or two excited electronic states, and only the bound configuration states in the ground and second excited electronic states. A classical approximation was used for the first excited electronic state, which had no bound configuration states. In addition, each many-electron transition matrix element was assumed to reduce to a product of single-electron matrix elements, so that the calculations were based on either a one-electron model or a one-electron model with multiple final system states.

Here we approach the problem differently. Our previous experience with $\chi^{(3)}$ calculations in $(CH)_x$ using a one-electron model with a classical fixed lattice[5] led us to conclude that ten or more electronic excited states must often be included in the sums for exact results, and five or more to ensure reliable results. For instance, we did some test calculations of $\chi^{(3)}$ for a 150-site chain of *trans*-$(CH)_x$ both with and without a medium-sized $S\bar{S}$ distortion, and limited the sums to only a few levels. If we summed over six valence levels but only one conduction level, we found a large increase in $\chi^{(3)}$ from the $S\bar{S}$. On the other hand, if we summed over two valence levels and two conduction levels, we found a sizable decrease in $\chi^{(3)}$ from the $S\bar{S}$. However, both of these cases gave $\chi^{(3)}$ spectra which were an order of magnitude smaller than that

obtained by including six valence levels and five conduction levels. Including more states than this in the sum only changes $\chi^{(3)}$ by about 5%, so the $\chi^{(3)}$ calculations in this paper used these limits. Since we are forced to include about 11 single-electron levels to obtain reliable results, and the computation scales as the fourth power of the number of states being summed over, it is necessary to keep the remainder of the calculation as simple as possible. We therefore use a one-electron model and a semiclassical treatment of the lattice. That is, we treat only the electronic ground state quantum mechanically. We ignore lattice quantization for the excited states, disregarding the effects of lattice-lattice wave-function overlaps in matrix elements. The value of an observable property is given in this method by

$$\mathcal{O}_{\text{semi}} = \int \mathcal{O}(h)P(h)dh \Big/ \int P(h)dh \ , \tag{2.10}$$

where $\mathcal{O}(h)$ is the value of the observable calculated for given h. For nonzero temperatures, the appropriate $P(h)$ is a Boltzmann-weighted average of the h probability for all lattice configuration states in the potential well arising from interaction with electrons in their ground state, given by

$$P(h) = \sum_i |\psi_i(h)|^2 e^{(E_i - E_0)/k_B T} \ , \tag{2.11}$$

where E_i and ψ_i are the energy and wave function, respectively, of the ith lattice configuration state [i.e., the ith solution of Eq. (2.6)]. However, for many calculations, the energy scale is such that $T \cong 0$ is sufficient at room temperature (i.e., only the lattice configuration ground state, $i = 0$, is needed). Such is the case in this paper.

We now describe our calculation of QLF effects on the first- and third-order absorption intensities, $\mathcal{I}^{(1)}$ and $\mathcal{I}^{(3)}$, respectively, in $(CH)_x$ in the $S\bar{S}$ approximation. (To a good approximation, $\mathcal{I}^{(3)}$ is proportional to the square of $\chi^{(3)}$, the magnitude of the third-order susceptibility. Since $\mathcal{I}^{(3)}$ is the observable, we report our results in this paper in terms of $\mathcal{I}^{(3)}$ rather than $\chi^{(3)}$.) First, we initialized the lattice by doping the system with two electrons from two donor impurities. The impurities were located 4 Å from the $(CH)_x$ chain and 12 sites apart. They contributed a Coulomb term to the electronic Hamiltonian. The system was allowed to relax self-consistently, which automatically induced the formation of an $S\bar{S}$, with the solitons pinned at the impurities. Keeping the lattice fixed, we removed the impurities and the extra electrons. This completed the lattice initialization stage. We recalculated the electronic energy levels and electronic wave functions, and used them to calculate the (classical) $\mathcal{I}^{(1)}$ and $\mathcal{I}^{(3)}$ spectra for a $(CH)_x$ chain with the given lattice configuration, as described in Appendix A. We also calculated the system energy $V(h)$, and "measured" $M(h)$ as explained above. We used the "height" of the distortion for h; this choice is explained below.

Subsequently, we allowed the lattice to relax dynamically to a different configuration. The S and $\bar{S}$ moved toward each other, diminishing h, attempting to cancel each other so that the lattice could return to its classical ground state. After each relaxation, we removed the lattice kinetic energy to ensure that we were mapping out the adiabatic potential well, calculated $V(h)$, and "measured" h and $M(h)$. We repeated this procedure until the distortion had almost disappeared. Negative distortions were obtained by reversing the positive distortions. We then solved Eq. (2.6) for the lowest-energy eigenvector. Lastly, we took the weighted average of the $\mathcal{I}^{(1)}$ and $\mathcal{I}^{(3)}$ spectra as in Eq. (2.10): we multiplied (classical) spectra calculated for $(CH)_x$ chains with given distortions by the (quantum) probabilities of the distortions, integrated this product over all distortions, and normalized by dividing by the integral of the probabilities over all distortions. This gave the desired semiclassical final result. Clearly, our procedure is easily varied for more complicated cases, other conducting and/or optically active polymers, other properties of interest, and other types of QLF's.

As their configurational coordinate, Yu, Matsuoka, and Su[13] and Sinclair *et al.*[6] chose the distance between the centers of the soliton and antisoliton. In our method, this was not measurable without fitting to an equation for the $S\bar{S}$, which violated the whole spirit of our "experimental" method. We attempted to use the full width at half maximum of the $S\bar{S}$ distortion, but surprisingly this did not change monotonically, and so was not useful. Instead, as our configuration coordinate, h, we chose the height of the $S\bar{S}$. (We define the height of the $S\bar{S}$ as the difference between the order parameter at the peak of the $S\bar{S}$ and the bulk order parameter of an undisturbed lattice.) Although we were somewhat forced into this choice of h by our method, Friedman and Su[14] made this same choice of h. They claimed that using the height for h gave better agreement with photoluminescence data than using the center separation, since positive and negative values of the height correspond to different $S\bar{S}$ distortions but positive and negative center separations do not.

In mapping out the potential well, we allowed the distortion to relax dynamically for 3 fs between points, using the method described in Appendix B. We used 0.2-fs time steps and set $U = 0$ in order to simplify the calculations. We show the resulting plots (for positive distortions) of potential energy vs distortion height and of effective mass vs distortion height in Figs. 1 and 2, respectively. The

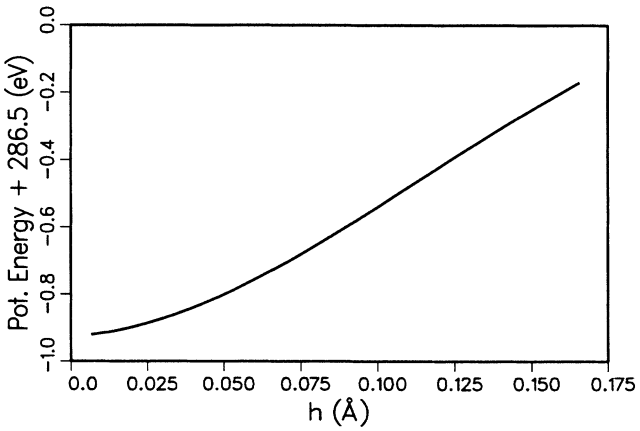

FIG. 1. System energy vs $S\bar{S}$ height.

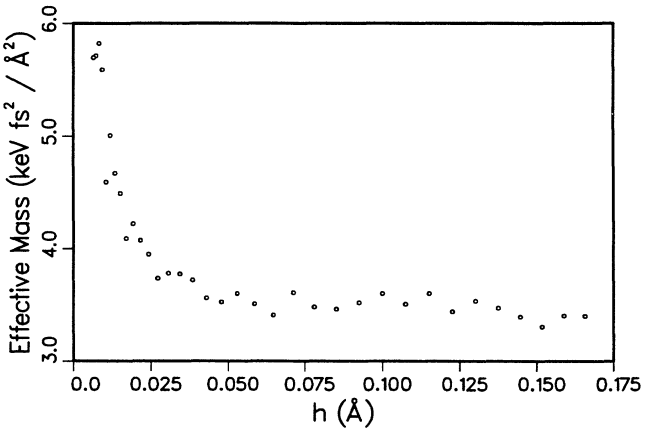

FIG. 2. Effective mass vs $S\bar{S}$ height.

jaggedness of the curve in Fig. 2 is probably simply an indication of the amount of "experimental error" in our "measurements" of the effective mass. Calculations showed that the plots are approximately symmetrical about zero height of the distortion, at least in the range of interest. It is reassuring that the effective mass is fairly constant over much of the range. In the equation used by Friedman and Su to approximate $S\bar{S}$ distortions, the effective mass is independent of the distortion height. On the other hand, the equation of Yu *et al.*, which is more exact but also more complicated, would clearly yield some sort of dependence on height (presumably similar to what we have obtained "experimentally"). We used spline interpolation between our known values of $V(h)$ and $M(h)$, and used a fourth-order Runge-Kutta method to solve Eq. (2.6), the Schrödinger equation with variable mass. The approximate symmetry about zero simplified this calculation from a boundary value problem to an initial value problem, since we knew the lowest-energy solution would be even. The lowest-energy eigenvector thus calculated is shown in Fig. 3. For all cases we made fixed lattice calculations of the absorption intensities for 18 $S\bar{S}$ heights, ranging from -0.145 to $+0.145$ Å. The probability of the maximum magnitude distortions was only 0.007 that of no distortions. The integrations in Eq. (2.10) were performed using spline quadrature.

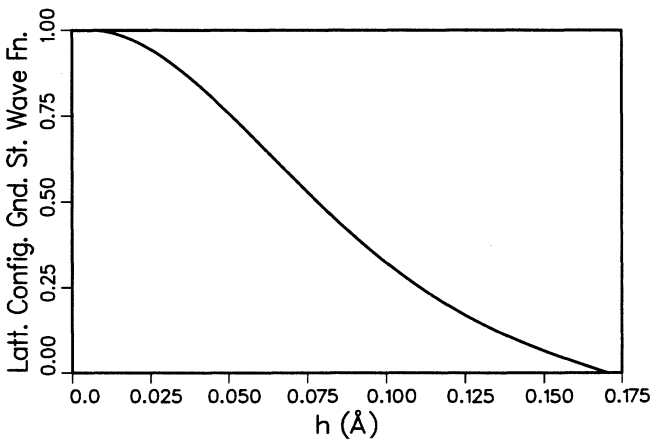

FIG. 3. Ground-state wave function.

III. RESULTS FOR POLYACETYLENE

Our first case is a long even chain (150 sites) of pristine *trans*-$(CH)_x$, with $S\bar{S}$ centers (i.e., the centers of the separation between the soliton and the antisoliton) at site 71, almost at the center of the chain. In Fig. 4, we show the relative intensity of the first-order absorption as a function of frequency, calculated ignoring QLF effects (dashed line) and including QLF effects in the $S\bar{S}$ approximation using the semiclassical method just described (solid line). (Note that the units for $\mathcal{I}^{(1)}$, although arbitrary, are consistent throughout this paper, in that all the figures omit the same multiplicative factor for $\mathcal{I}^{(1)}$.) The low-energy broadening of the interband absorption peak, first attributed to QLF effects by Yu, Matsuoka, and Su[13] and more recently to a combination of QLF and thermal effects by McKenzie and Wilkins,[15] is successfully reproduced by the semiclassical method. This broadening would be more pronounced if one averaged only over positive height distortions, which is effectively what was done by Yu, Matsuoka, and Su. Alternatively, one could make use of the slight increase in the average band gap, visible in Fig. 4, caused by negative height distortions. By varying Hamiltonian parameters, one could reduce the classical band gap for the QLF case in order to shift the solid line to lower energies so that the interband edges would line up, and thus, in effect, increase the absorption at each frequency in the low-energy region.

We found that centered $S\bar{S}$'s had very little effect on the third-order absorption intensity. However, Fig. 5 shows the calculated relative intensity of the third-order absorption as a function of frequency, without QLF effects (dashed line) and with QLF effects (solid line), for a 150-site chain with $S\bar{S}$'s away from the chain center (centered at site 41). (As in first order, note that the units for $\mathcal{I}^{(3)}$, although arbitrary, are consistent throughout

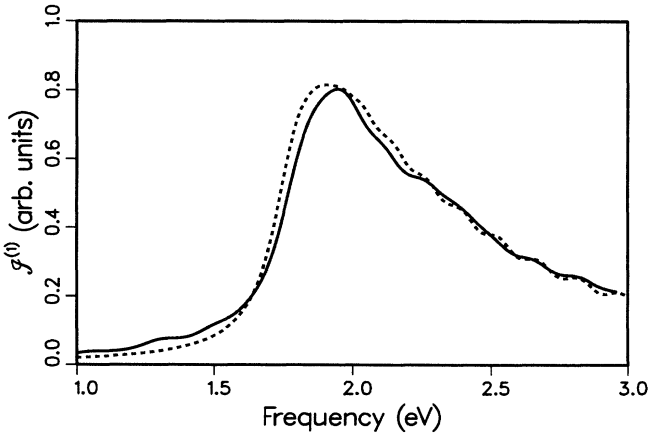

FIG. 4. First-order absorption: Even *trans*, $S\bar{S}$'s centered. Relative intensity of the first-order absorption as a function of frequency, for a 150-site chain with the $S\bar{S}$'s always centered at site 71, calculated ignoring QLF effects (dashed line) and including QLF effects (solid line).

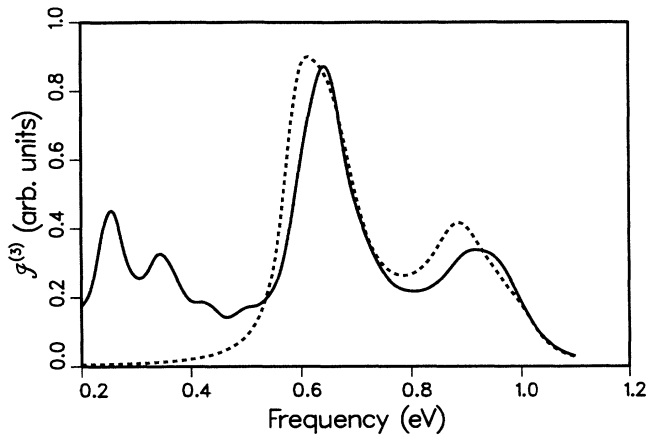

FIG. 5. Third-order absorption: Even *trans*, $S\bar{S}$'s off center. Relative intensity of the third-order absorption as a function of frequency, for a 150-site chain with the $S\bar{S}$'s centered at site 41, calculated ignoring QLF effects (dashed line) and including QLF effects (solid line).

this paper.) We find a large increase and an $S\bar{S}$ peak structure in $\mathcal{I}^{(3)}$ below the usual interband three-photon peak at 0.6 eV. The peak structure is the result of the tradeoff between increasing $\mathcal{I}^{(3)}$ and decreasing probability, for increasing $S\bar{S}$ heights. The peaks are spread out because there is a range over which the tradeoff is fairly constant but the $S\bar{S}$ energy levels are changing. As expected, we found that the QLF effects on the first-order absorption were not changed by moving the $S\bar{S}$'s away from the chain center. For the remaining cases, we report results only for $S\bar{S}$'s centered away from the chain center (at site 41), and for undistorted chains.

Our second case is a long odd chain (149 sites) of pristine *trans*-$(CH)_x$ with the neutral soliton centered on the chain (at site 75), and with uncentered $S\bar{S}$'s. In Fig. 6, we show the relative intensity of the first-order absorption as a function of frequency, calculated ignoring QLF effects (dashed line) and including QLF effects (solid line). We see two interesting QLF effects, both due to $S\bar{S}$'s with negative heights. The soliton peak is flattened and spread out toward higher energy, while the main band has acquired a double peak. The higher-energy peak is due to a range of heights with a favorable tradeoff between increased QLF effects and decreased probability, as above. Keep in mind that $U=0$ in these calculations. As we stated earlier, for $U=4$ the soliton peak appears at a higher energy, within the tail of the main band. Here we see that QLF effects will further decrease the chances of resolving the soliton peak.

Figure 7 shows the calculated relative intensity of the third-order absorption as a function of frequency for this case, without QLF effects (dashed line) and with QLF effects (solid line). As for even chains, we find a large increase and a peak structure in $\mathcal{I}^{(3)}$ below the three-photon peak at 0.6 eV. The neutral soliton peak seen in the classical lattice calculation is obscured by the QLF effects. However, the soliton state seems to augment the QLF effects at the expense of the classical peaks. The magnitude of the interband peaks is reduced by half, and the interband two-photon peak is clearly split into a lower-energy peak due to positive height $S\bar{S}$'s and a higher-energy peak due to negative height $S\bar{S}$'s.

Our third case is a long odd chain (149 sites) of pristine *trans*-$(CH)_x$ with the neutral soliton off center towards one end of the chain (at site 115) and the $S\bar{S}$'s off center towards the other end (as above). The first-order optical absorption spectrum is the same as in the second case. The third-order absorption results are quite different, and are shown in Fig. 8, where the dashed line is for the classical lattice results (no $S\bar{S}$'s) and the solid line is for results including QLF effects. With no $S\bar{S}$'s, the relative intensity has very large, clear soliton three-photon and two-photon peaks below the interband three-photon and two-photon peaks. These soliton peaks are actually de-

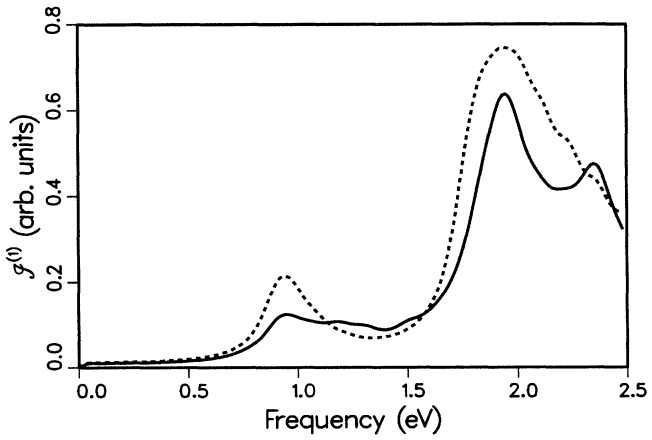

FIG. 6. First-order absorption: Odd *trans*, $S\bar{S}$'s off center, S^0 centered. Relative intensity of the first-order absorption as a function of frequency, for a 149-site chain with $S\bar{S}$ centers at site 41 and the S^0 center at site 85, calculated ignoring QLF effects (dashed line) and including QLF effects (solid line).

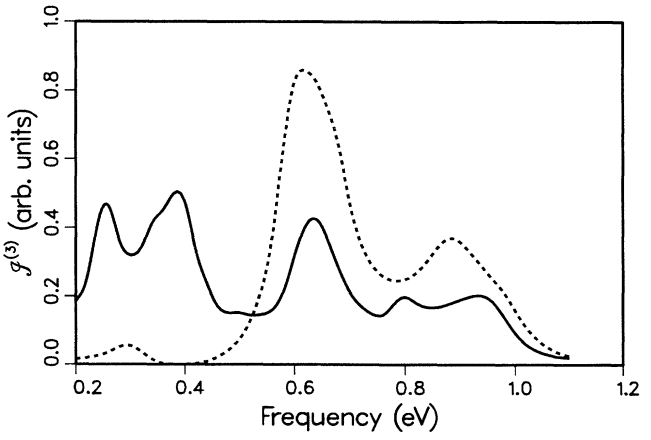

FIG. 7. Third-order absorption: Odd *trans*, $S\bar{S}$'s off center, S^0 centered. Relative intensity of the third-order absorption as a function of frequency, for a 149-site chain with $S\bar{S}$ centers at site 41 and the S^0 center at site 85, calculated ignoring QLF effects (dashed line) and including QLF effects (solid line).

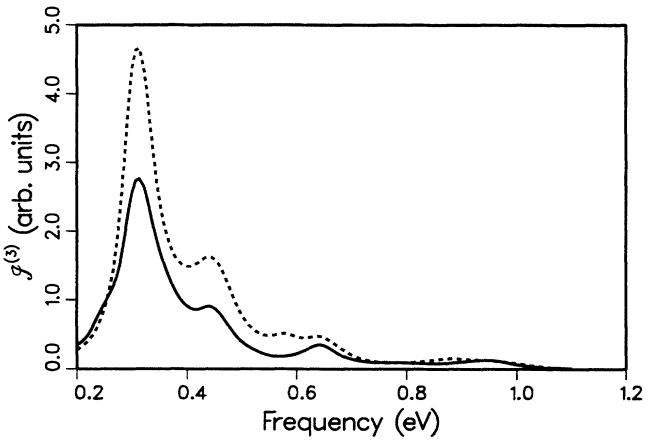

FIG. 8. Third-order absorption: Odd *trans*, $S\bar{S}$'s and S^0 off center. Relative intensity of the third-order absorption as a function of frequency, for a 149-site chain with $S\bar{S}$ centers at site 41 and the S^0 center at site 115, calculated ignoring QLF effects (dashed line) and including QLF effects (solid line).

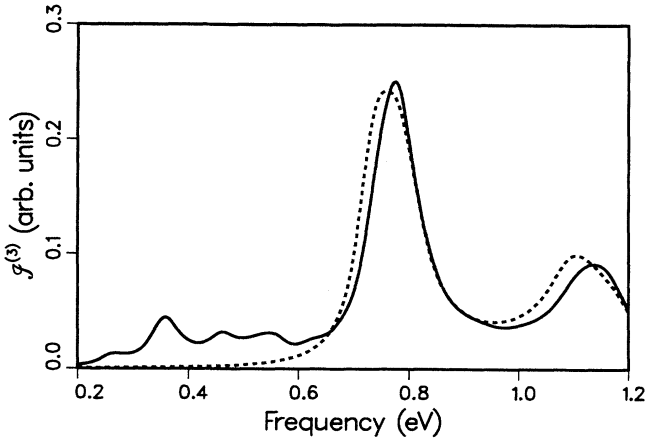

FIG. 10. Third-order absorption: *cis*, $S\bar{S}$'s off center. Relative intensity of the third-order absorption as a function of frequency, for a 150-site *cis* chain with $S\bar{S}$ centers at site 41, calculated ignoring QLF effects (dashed line) and including QLF effects (solid line).

creased by the $S\bar{S}$'s, possibly due to increased disorder. There are competing effects: more asymmetric electronic states cause $\mathcal{I}^{(3)}$ to increase, but more disorder causes $\mathcal{I}^{(3)}$ to decrease.

We turn now to the other polyacetylene isomer, *cis*-$(CH)_x$. We modeled it by adding an off-diagonal symmetry breaking term,

$$g\sum_{n,s}(-1)^n(C^{\dagger}_{n+1,s}C_{n,s}+C^{\dagger}_{n,s}C_{n+1,s})\ , \tag{3.1}$$

to the Hamiltonian used for *trans*-$(CH)_x$ (see Appendix B), as suggested by Brazovskii and Kirova.[16] The value of g is set so that the calculated first-order optical absorption spectrum matches the experiment. We found that $g=-0.05$ eV gave reasonable agreement with measurements.[17] Our next task was to find $V(h)$ and $M(h)$; however, a full calculation turned out to be unnecessary. Preliminary calculations showed that $V(h)$ and $M(h)$ for *cis*-$(CH)_x$ are roughly similar to those obtained for *trans*-$(CH)_x$ for the values of h in which we are interested in this investigation. We therefore used the wave function shown in Fig. 3 to weight our *cis* results as well as our *trans* results.

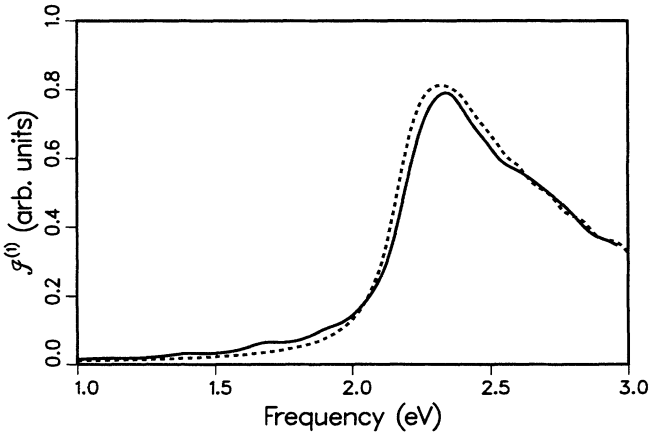

FIG. 9. First-order absorption: *cis*, $S\bar{S}$'s off center. Relative intensity of the first-order absorption as a function of frequency, for a 150-site *cis* chain with $S\bar{S}$ centers at site 41, calculated ignoring QLF effects (dashed line) and including QLF effects (solid line).

Our results for the relative intensity of the first-order absorption as a function of frequency, calculated ignoring QLF effects (dashed line) and including QLF effects (solid line), are shown in Fig. 9, for a 150-site *cis* chain with $S\bar{S}$'s away from the chain center (centered at site 41). There is a slight broadening in the low-energy tail of the interband peak, as for an even *trans* chain. Note that the band gap is larger for *cis*-$(CH)_x$ than for *trans*-$(CH)_x$. Figure 10 shows the calculated relative intensity of the third-order absorption as a function of frequency, without QLF effects (dashed line) and with QLF effects (solid line). As for an even *trans* chain, we find an increase and an $S\bar{S}$ peak structure in $\mathcal{I}^{(3)}$ below the interband three photon peak at 0.6 eV. However, the QLF effects are smaller for *cis*-$(CH)_x$. Also, $\mathcal{I}^{(3)}$ for *cis*-$(CH)_x$ is generally only about one-fourth that for *trans*-$(CH)_x$, and the peaks are at slightly higher energies due to the larger band gap.

IV. CONCLUSION

We have presented a method of accounting for the effects on the properties of linear polymers of those classes of quantum lattice fluctuations which are definable with a single configuration coordinate. We have applied this method to soliton-antisoliton pairs in polyacetylene. Our results for the first-order optical absorption of even *trans* chains are in substantial agreement with an earlier calculation,[13] which used a different method and a different configurational coordinate. We

find that the first-order absorption is insensitive to the position of the $S\bar{S}$'s along the chain, but that the QLF effects on the third-order absorption are greatly enhanced by moving the $S\bar{S}$'s away from the chain center. It seems clear that any attempt to incorporate QLF effects realistically into calculations of nonlinear optical properties of quasi-one-dimensional polymers must include averaging over possible locations of the QLF's along the chain. We have seen that even far off-center $S\bar{S}$'s can sometimes suppress the main band of the $\mathcal{I}^{(3)}$ spectrum, showing the sensitivity of the nonlinear optical properties of polymers to disorder. We find that the effects of $S\bar{S}$'s on $\mathcal{I}^{(3)}$ of $(CH)_x$ are most important in the region below the interband three-photon peak. For materials with "empty" band gaps, it is likely that QLF's are the main cause of any low-frequency nonlinear responses. Lastly, our calculations on *cis*-$(CH)_x$ indicate that QLF effects on nonlinear optical properties may be important even for materials with a nondegenerate ground state.

APPENDIX A: INTENSITY CALCULATIONS

We first diagonalize the Hamiltonian matrix (see Appendix B) to obtain the one-electron energies and wave functions. A Kubo-type calculation gives the conductivity in terms of a density-current correlation function. Evaluating this function gives the site-averaged conductivity

$$\sigma(\omega)=(i/\hbar)\frac{e^2a}{N}\sum_{\alpha,\beta}\frac{|W_{\alpha\beta}|^2\omega_{\alpha\beta}[n_F(E_\beta)-n_F(E_\alpha)]}{\omega-\omega_{\alpha\beta}+i\eta}\ , \tag{A1}$$

where α and β index single-particle states and the summation is taken over all states for each index. $W_{\alpha\beta}$ is a dipole matrix element, $\omega_{\alpha\beta}$ is the difference in energy between states α and β, and $n_F(E_\alpha)$ is a Fermi factor. The input frequency (in eV) is denoted by ω, and η is a phenomenological damping factor. (For the calculations reported here, we have chosen $\eta=0.09$ eV on empirical grounds by varying η for a dimerized chain so as to reproduce the shape of the $\chi^{(3)}$ spectrum found for pure samples.)

Once the conductivity of a single chain is known, one can find the dynamic dielectric constant of a film using

$$\varepsilon(\omega)=\varepsilon_0+4\pi i\rho_c\sigma(\omega)/\omega\ , \tag{A2}$$

where ρ_c is the density of chains per unit cross-sectional area. We assume $\rho_c=7\times10^{14}$ cm^{-2}, corresponding to a lattice of $(CH)_x$ chains each separated by about 4 Å.

The absorption coefficient for decay of an electromagnetic wave passing through the medium is given by twice the imaginary part of the propagation vector

$$2K=\sqrt{2}(\omega/c)[|\varepsilon(\omega)|-\varepsilon_1(\omega)]^{1/2}\ , \tag{A3}$$

where the subscript 1 indicates the real part. For a thin film, this is approximately proportional to the first-order absorption intensity

$$\mathcal{I}^{(1)}\equiv\mathcal{I}_0-\mathcal{I}_f=\mathcal{I}_0[1-e^{-2Kd}]\cong\mathcal{I}_0 2Kd\ . \tag{A4}$$

Further details are given in Ref. 12.

The third-order susceptibility is obtained from perturbation theory about the adiabatic ground state (see, for example, Refs. 18 and 19) and is given by

$$\begin{aligned}\chi^{(3)}\propto\sum W_{\alpha\beta}W_{\beta\gamma}W_{\gamma\delta}W_{\delta\alpha}n_F(E_\alpha)\Bigg[&\frac{1}{(\omega+\omega_{\alpha\beta}+i\eta)(2\omega+\omega_{\alpha\gamma}+i2\eta)(3\omega+\omega_{\alpha\delta}+i3\eta)}\\&+\frac{1}{(-\omega+\omega_{\alpha\beta}-i\eta)(-2\omega+\omega_{\alpha\gamma}-i2\eta)(-3\omega+\omega_{\alpha\delta}-i3\eta)}\\&+\frac{1}{(\omega+\omega_{\alpha\beta}+i\eta)(-2\omega+\omega_{\alpha\gamma}-i2\eta)(-3\omega+\omega_{\alpha\delta}-i3\eta)}\\&+\frac{1}{(-\omega+\omega_{\alpha\beta}-i\eta)(2\omega+\omega_{\alpha\gamma}+i2\eta)(3\omega+\omega_{\alpha\delta}+i3\eta)}\Bigg]\ .\end{aligned} \tag{A5}$$

Since each dipole matrix element W requires N multiplications, and there are N^4 combinations of W's in Eq. (A5), the calculation scales as N^5. However, by clever nesting of do-loops, calculating all of the W's once and storing them, and using both the parity of the states and features of the magnitudes of the W's to restrict the sums, the calculations can be done in reasonable times even for very long chains. Further details are given in Refs. 5 and 18.

APPENDIX B: DYNAMICS OF THE $(CH)_x$ LATTICE

In this appendix we explain our method of calculating the dynamics of the $(CH)_x$ lattice, which we have used in several studies.[20] We start with the Born-Oppenheimer approximation. We also assume the lattice sites are massive enough that, to first order, we can safely ignore quantum effects in our dynamics calculations. While quantum effects in $(CH)_x$ are not negligible (hence this

paper; see also Refs. 21 and 22), they are sufficiently small to enable us to conclude, *via* Ehrenfest's theorem, that they will occur in the form of fluctuations about the classical trajectory. Therefore, we move the lattice according to classical equations of motion, in which the force on a site depends both on the relative positions of nearest-neighbor sites and on the electronic wave functions.

To describe one of the chains making up $(CH)_x$ we use the Su-Schrieffer-Heeger Hamiltonian,[23] usually augmented by an on-site Hubbard (electron interaction) term treated in the mean-field approximation.[24] The π electrons are described by the Hamiltonian

$$\begin{aligned} H_{\text{elec}} = & -\sum_{n,s}[t_0+\alpha(u_{n+1}-u_n)] \\ & \times(C^{\dagger}_{n+1,s}C_{n,s}+C^{\dagger}_{n,s}C_{n+1,s}) \\ & +U\sum_{n,s}C^{\dagger}_{n,s}C_{n,s}(\langle C^{\dagger}_{n,-s}C_{n,-s}\rangle-\tfrac{1}{2}) \\ & +\sum_{n,s}V_nC^{\dagger}_{n,s}C_{n,s}\ , \end{aligned} \tag{B1}$$

where the sums are over sites and spins. The lattice Hamiltonian is

$$\begin{aligned} H_{\text{latt}} = & \tfrac{1}{2}M\sum_n(\dot{u}_n)^2 \\ & -\alpha\sum_{n,s}(u_{n+1}-u_n)(C^{\dagger}_{n+1,s}C_{n,s}+C^{\dagger}_{n,s}C_{n+1,s}) \\ & +\tfrac{1}{2}K\sum_n(u_n-u_{n+1})^2\ . \end{aligned} \tag{B2}$$

In the above equations, $C^{\dagger}_{n,s}$ and $C_{n,s}$ are creation and annihilation operators, respectively, for an electron in a π orbital on site n with spin s. The displacement of the nth lattice site from its equilibrium position is represented by u_n, and the mass of a site (13 amu) is given by M. The intrachain hopping parameter is t_0, the strength of the change in hopping due to the electron-phonon interaction is denoted by α, the strength of the σ bond "springs" is determined by K, and U is the on-site Hubbard electron interaction parameter. V_n is an optional impurity potential. The values which we use for the parameters are $t_0=2.5$ eV, $\alpha=4.37$ eV/Å, and $K=21$ eV/Å^2. Generally, one would vary U from 0 to 4 eV; however, in this paper we always used $U=0$ to simplify the calculations. Note that the electron-phonon interaction term has been included in both H_{elec} and H_{latt}, so that the total Hamiltonian is not the sum of these terms. Note also that, if the last term in H_{elec} is a Coulomb term, then it should, in principle, be included in H_{latt} also, since it contains a u_n dependence. However, in practice, the π band charge due to the impurity has a high probability of occupying the sites near the impurity. This screens the impurity, so that its net direct effect on the lattice is small even for sites near the excited site.

To find the forces on the lattice sites, we use the Feynman-Hellman theorem

$$F_n=-\left\langle\psi\left|\frac{\partial H}{\partial u_n}\right|\psi\right\rangle\ , \tag{B3}$$

which leads to the equations of motion

$$Md^2u_n/dt^2=K(u_{n+1}+u_{n-1}-2u_n)-KQ_n \tag{B4}$$

for $n=2$ to $N=1$, with the usual modifications for $n=1$ and N. For boundary conditions, we set $u_1=u_N=0$, which are the same boundary conditions used in our equilibrium calculations.[25] In the above equations,

$$Q_n=(2\alpha/K)\sum_{k,s}(A^{k,s}_nA^{k,s}_{n+1}-A^{k,s}_nA^{k,s}_{n-1})\ , \tag{B5}$$

where k runs from 1 to $N/2$, and where $A^{k,s}_n$ stands for the probability amplitude of site n being occupied by an electron in level k with spin s. Note that $A^{k,s}_0=A^{k,s}_{N+1}=0$. Exact solutions to Eqs. (B4) and (B5) are not difficult to obtain if the values of $A^{k,s}_n$ are known. Various schemes have been devised[26,27] for doing lattice dynamics calculations without $A^{k,s}_n$ and the attendant large matrices; however, we often needed $A^{k,s}_n$ for our calculations, so this option was not utilized. The complementary solutions (i.e., the solutions to the homogeneous equation) for the given boundary conditions are well known,[28] and the particular solutions, $\mathcal{P}_n$, are just constants satisfying the matrix equation

$$\mathcal{P}_{n+1}+\mathcal{P}_{n-1}-2\mathcal{P}_n=Q_n\ , \tag{B6}$$

so that the complete solutions are

$$\begin{aligned} u_n(t)= & \sum_{r=1}^{N-2}\sin(n\gamma_r-\gamma_r) \\ & \times[a_r\sin(\omega_rt)+b_r\cos(\omega_rt)]+\mathcal{P}_n\ , \end{aligned} \tag{B7}$$

where a_r and b_r are constants determined by initial conditions, and where

$$\omega_r=2(K/M)^{1/2}\sin(\gamma_r/2)\ , \tag{B8a}$$

$$\gamma_r=r\pi/(N-1)\ . \tag{B8b}$$

We alternately allow the lattice to move and find the new electronic ground states, assuming that the electronic forces on the lattice do not change significantly over short time steps. In order to determine the appropriate time step, preliminary calculations are done with various time steps, and the resultant lattice dynamics and total energies are compared.

[1]A. J. Heeger, S. Kivelson, J. R. Schrieffer, and W.-P. Su, Rev. Mod. Phys. **60**, 781 (1988).
[2]F. Kajzar, S. Etemad, G. L. Baker, and J. Messier, Synth. Met. **17**, 563 (1987).
[3]W. S. Fann, S. Benson, J. Madey, S. Etemad, G. L. Baker, and F. Kajzar, Phys. Rev. Lett. **62**, 1492 (1989).
[4]M. R. Drury, Solid State Commun. **68**, 417 (1988).
[5]D. M. Mackie, R. J. Cohen, and A. J. Glick, Phys. Rev. B **39**, 3442 (1989).
[6]M. Sinclair, D. Moses, D. McBranch, A. J. Heeger, J. Yu, and

W.-P. Su, Synth. Met. **28**, 655 (1989).
[7]W. Wu, Phys. Rev. Lett. **61**, 1119 (1988).
[8]J. Yu, B. Friedman, P. R. Baldwin, and W.-P. Su, Phys. Rev. B **39**, 12 814 (1989).
[9]C. Wu and X. Sun, Phys. Rev. B **41**, 12 845 (1990).
[10]C. Wu and X. Sun, Phys. Rev. B **42**, 9736 (1990).
[11]C. Singh and D. Hone, Synth. Met. (to be published).
[12]A. J. Glick and G. W. Bryant, Phys. Rev. B **34**, 943 (1986); A. J. Glick, R. J. Cohen, and G. W. Bryant, *ibid.* **37**, 2653 (1988).
[13]J. Yu, H. Matsuoka, and W.-P. Su, Phys. Rev. B **37**, 10 367 (1988).
[14]B. Friedman and W.-P. Su, Phys. Rev. B **39**, 5152 (1989).
[15]R. McKenzie and J. W. Wilkins, Phys. Rev. Lett. **69**, 1085 (1992).
[16]S. A. Brazovskii and N. Korova, Pis'ma Zh. Eksp. Teor. Fiz. **33**, 6 (1981) [JETP Lett. **33**, 4 (1981)].
[17]D. C. Bott, in *Handbook of Conducting Polymers,* edited by T. A. Skotheim (Dekker, New York, 1986), Vol. 2, p. 1204.
[18]N. Bloembergen, *Nonlinear Optics* (Benjamin, New York, 1965).
[19]D. C. Hanna, M. A. Yuratich, and D. Cotter, *Nonlinear Optics of Free Atoms and Molecules* (Springer-Verlag, Berlin, 1979).
[20]D. M. Mackie, Doctoral dissertation, University of Maryland at College Park, 1991, University Microfilm International, No. AAD92-22725.
[21]W.-P. Su, S. Kivelson, and J. R. Schreiffer, in *Physics in One Dimension,* edited by T. Bernasconi and T. Schneider (Springer, Berlin, 1980), p. 201.
[22]J. E. Hirsch and E. Fradkin, Phys. Rev. B **27**, 1680 (1983); **27**, 4302 (1983); J. E. Hirsch, R. L. Sugar, D. J. Scalapino, and R. Blankenbeckler, *ibid.* **26**, 5033 (1982).
[23]W.-P. Su, J. R. Schrieffer, and A. J. Heeger, Phys. Rev. Lett. **42**, 1698 (1979); Phys. Rev. B **22**, 2099 (1980).
[24]C. Wu and X. Sun, Phys. Rev. B **33**, 8772 (1986).
[25]R. J. Cohen and A. J. Glick, Phys. Rev. B **36**, 2907 (1987); R. J. Cohen, Doctoral dissertation, University of Maryland at College Park, 1991, University Microfilm International, No. AAD92-22670.
[26]F. Guinea, Phys. Rev. B **30**, 1884 (1984).
[27]S. R. Phillpot, D. Baeriswyl, A. R. Bishop, and P. S. Lomdahl, Phys. Rev. B **35**, 7533 (1987).
[28]J. B. Marion, *Classical Dynamics of Particles and Systems,* 2nd ed. (Academic, New York, 1970).